# Preliminary Experimental Study of Methane Adsorption Capacity in Shale After Brittle Deformation Under Uniaxial Compression

Mingliang Liang[1,2,3]*, Zongxiu Wang[1,2]*, Guodong Zheng[4], Xiaobao Zhang[4], Hugh Christopher Greenwell[3], Kaixun Zhang[1,2], Xingqiang Feng[1,2], Linyan Zhang[1,2] and Huijun Li[1,2]

[1] Institute of Geomechanics, Chinese Academy of Geological Sciences, Beijing, China, [2] Key Laboratory of Petroleum Geomechanics, China Geological Survey, Beijing, China, [3] Department of Earth Sciences, Durham University, Durham, United Kingdom, [4] Key Laboratory of Petroleum Resources, Gansu Province, Northwest Institute of Eco-Environment and Resources, Chinese Academy of Sciences, Lanzhou, China

This paper presents a preliminary experimental study on methane adsorption capacity in shales before and after artificial deformation. The experimental results are based on uniaxial compression and methane isothermal adsorption tests on different shale samples from the Silurian Longmaxi Formation, Daozhen County, South China. Two sets of similar cylindrical samples were drilled from the each same bulk sample, one set was subjected to a uniaxial compressive simulation test and then crushed as artificial deformed shale sample, the other set was directly crushed as the original undeformed shale sample. And then we conducted a comparative experimental study of the methane adsorption capacity of original undeformed and artificially deformed shales. The uniaxial compression simulation results show that the failure mode of all samples displayed brittle deformation. The methane isothermal adsorption results show that the organic matter content is the main controlling factor of shale methane adsorption capacity. However, the comparative results also show that the compression and deformation have an effect on methane adsorption capacity, with shale methane adsorption capacity decreasing by about 4.26–8.48% after uniaxial compression deformation for the all shale samples in this study.

Keywords: methane adsorption capacity, Longmaxi Shale, uniaxial compressive, brittle deformation, TOC

## INTRODUCTION

The adsorbed gas accounts for a large proportion of the total shale gas content and has a significant impact on shale gas resource potential (Ross and Bustin, 2009; Zhang et al., 2012; Wu et al., 2014; Vishal et al., 2019). For example, in the Devonian shale in the Appalachian basin, United States, the adsorbed gas content has been shown to be higher than 50% of the total gas in place (Lu et al., 1995). Ross and Bustin (2009), indicated that the adsorbed gas accounts for 20–85% of total gas for the Antrim, Ohio, New Albany, Barnett, and Lewis shale gas plays. In non-USA based shale systems, based on the raw data from the Changning and Jiaoshiba gas fields, we could calculated that the adsorbed gas accounts for 20–40% of total gas content of the Longmaxi shale (Wang et al., 2016).

In order to determine the amount of adsorbed methane ($CH_4$) on shale samples, previous studies have performed $CH_4$ sorption capacity measurements (Ross and Bustin, 2007, 2008, 2009; Chalmers and Bustin, 2008a,b; Zhang et al., 2012; Tan et al., 2014; Psarras et al., 2017; He et al., 2019; Wei et al., 2019). The $CH_4$ adsorption capacity in shale samples has been widely recognized as varying significantly depending upon the composition (organic matter and clay mineral type and amount) of the shales, as well as the physical porosity and pore properties (Hill et al., 2007; Javadpour et al., 2007; Ross and Bustin, 2007, 2008, 2009; Chalmers and Bustin, 2008a,b; Jenkins and Boyer, 2008; Zhang et al., 2012; Hou et al., 2014; Tan et al., 2014; He et al., 2019; Tang et al., 2019; Jiang et al., 2020). Thus, an understanding of the relationships between organic matter (type, maturity and content), clay mineral (type and content), porosity (microporous structural framework) and methane sorption capacity in shale is crucial for assessing the shale reservoir.

The organic matter (OM) content is the first key factor that determines the gas adsorption capacity of shale (Hill et al., 2007; Mastalerz et al., 2012). Positive correlations are reported between methane sorption capacity and both total organic carbon (TOC) and micropore (<2 nm) volume in shale, indicating micropores associated with the OM are a significant factor controlling gas adsorption (Chalmers and Bustin, 2007; Ross and Bustin, 2007, 2009; Tan et al., 2014). Guo et al. (2017) studied samples from the Mesozoic shales in the Tarim Basin, observing that the $CH_4$ adsorption capacity increased with increasing TOC content. By studying the relationship between $CH_4$ sorption capacity and pore characteristics of shales from the Baltic Basin, Poland, Topór et al. (2017) found that $CH_4$ adsorption in was predominantly controlled by the OM micropore structure. Comparative experiments of methane adsorption on both original shale samples and isolated kerogen were conducted by Zhang et al. (2012), with the total amount of methane adsorbed directly proportional to the TOC content and an average maximum $CH_4$ sorption of 1.36 mmol.g$^{-1}$ TOC. Yang et al. (2016) found that $CH_4$ sorption capacity increased with the TOC content, surface area and micropore volume, suggesting OM provided abundant adsorption surfaces, as well as pore space, and enhanced the $CH_4$ sorption capacity. Moreover, the type of OM and its thermal maturity (usually defined by Ro%) are also known to influence the $CH_4$ sorption capacity of shales (Lu et al., 1995; Hill et al., 2004; Zhang et al., 2012). Based on $CH_4$ adsorption experiments of shale samples with different Ro%, Zhang et al. (2012) found that those kerogen types with a greater degree of aromatization have higher gas adsorbing capacity than those with aliphatic structures, leading to Langmuir pressure ($P_L$) changes according to kerogen type in the sequence of Type I > Type II > Type III. However, compared to the Longmaxi Shale, and other shales, that display Ro% less than 3.0%, Li et al. (2017) argued that the Niutitang shales, with Ro% higher than 4.0% have lower methane adsorption capacity. Similarly, Topór et al. (2017) also observed that $CH_4$ adsorption potential decreases in micropores with increasing maturity of shales from the Baltic Basin, Poland.

Clay minerals also influence the methane adsorption capacity of shale, especially for organic-lean shale deposits, with low TOC. Cheng and Huang (2004) pointed out that many clay minerals consist of porous aggregates and structures, providing larger surface areas and more potential adsorption sites than other minerals. Ji et al. (2012) observed that methane adsorption capacity showed significant differences with different clay minerals, as $CH_4$ sorption capacity decreases in the order montmorillonite > I–S mixed layer > kaolinite > chlorite > illite. To try and understand adsorption at mixed mineral-OM interfaces, a study of gas adsorption in organic-inorganic pores made in graphene – montmorillonite composites, as a model shale matrix, by Chen et al. (2020) found that the graphene (OM) surface shows a significantly stronger adsorption capacity than the graphene – montmorillonite, though this decreased with increasing pressure.

As well as shale composition affecting the $CH_4$ adsorption, there are also environmental effects. Considerable *in situ* and experimental work has been performed on understanding the gas adsorption capacity of shale with environmental factors including the effect of moisture (Zou et al., 2018), high pressure (Li et al., 2016) and particle size (Gao et al., 2018), contributing to the wider understanding of the adsorption characteristics of shales. While the adsorption of $CH_4$ at nanopores and their associated surface area in shale is controlled by shale matrix composition (OM and mineral content) and geological environmental conditions, it is also affected by tectonic stress and structural deformation (Ma et al., 2015; Liang et al., 2017; He et al., 2018; Wang, 2020; Zhu et al., 2020). Aplin et al. (2006) reported that the microstructure and pore properties of Mexican mudstones changed due to mechanical compaction. Based on uniaxial and/or triaxial compression experiments, several studies have been conducted on the deformational behavior, microstructure and pore/fracture evolution of shale (Arora and Mishra, 2015; Mishra and Verma, 2015; Minaeian et al., 2017; Wang and Li, 2017; Wang et al., 2018; Bakhshian and Hosseini, 2019; Liu et al., 2019; Tan et al., 2019), with microstructure, pore properties and permeability all influenced by compression and deformation. Using artificial compaction to make pellets of Wyoming montmorillonite powder, (Kuila and Prasad, 2013) found that compaction could results in decrease in pore volume and reduction of macropores of the clays. However, to our knowledge, hitherto the effect of compressive deformation on the $CH_4$ adsorption capacity of shale has received little attention.

With the progress of shale gas research in tectonically deformed areas in southern China, studies have been conducted using natural deformation shale (Ma et al., 2015, 2020; Liang et al., 2017; Zhu et al., 2020) and numerical simulation (Wei et al., 2019). Researchers have recognized that stress deformation has effect on shale adsorption capacity, but whether the relationship between stress deformation and adsorption capacity is promoting (Ma et al., 2015, 2020) or depressing (Wei et al., 2019; Zhu et al., 2020) is still unclear. In this paper we present an experimental study of uniaxial compression induced brittle deformation and its influence on the methane adsorption capacity of shale. The main purpose of the study was to investigate whether or not compression impacted $CH_4$ adsorption capacity of shale and, if so, quantify the scale of the change in adsorption capacity.

**FIGURE 1 |** Map showing the location and outcrop photograph of study area in Daozhen, Guizhou province, Southern China. $S_1l$- Lower Silurian Longmaxi Formation, $O_3b$- Upper Ordovician Baota Formation.
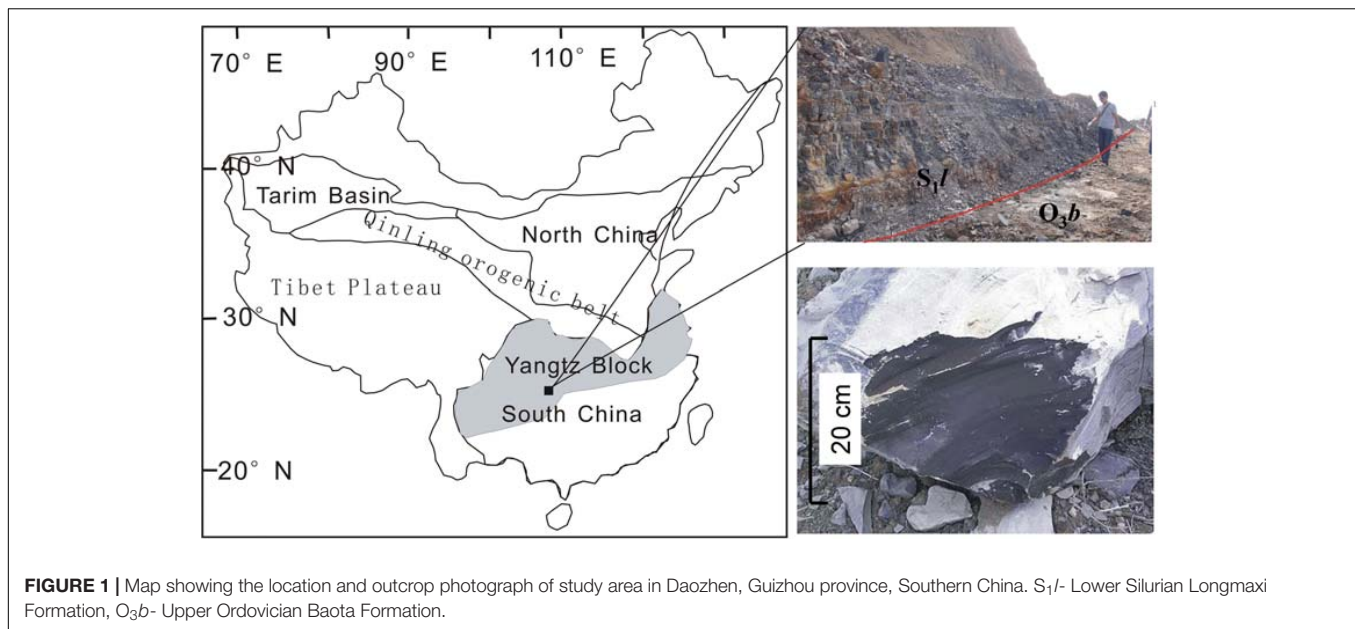
## MATERIALS AND METHODS

### Shale Samples and Sample Preparation

Five bulk shale samples were collected from outcrops of the Longmaxi formation. For research purposes, the shale samples are undeformed shale, and no fractures or vein are observed on the hand scale. The sampling site in Daozhen County is located in the North of Guizhou province, which belongs to the edge of the Upper Yangtze Block (28°53′46″N, 107°31′48″E; **Figure 1**). Two similar cylindrical samples of about 25 mm diameter and 20–50 mm length were obtained from each bulk sample, of which one was used in a uniaxial compressive simulation experiment and denoted as the artificial deformed shale sample (D), the other was denoted as the original shale sample (O). And then we got 10 shale samples for methane adsorption capacity tests. All samples were crushed into 0.25 mm (60 mesh) size samples as per the GB/T 19560–2004 testing standard (China National Standard), prepared for methane adsorption capacity measurements. The remaining material from 5 bulk samples were collected and powdered to 200 mesh particle sizes for geochemical (TOC) and mineralogical composition analysis using X-ray diffraction (XRD) analysis. The TOC content was measured with a Leco C/S-344 analyzer after samples were treated with 10% hydrochloric acid to remove carbonate. The mineral composition was measured using a D/Max-III analyzer for X-ray diffraction (XRD) analysis. All the data were obtained under the same sample preparation, analytical models and calculation models for both artificial brittle deformed and original samples, except whether it has experienced uniaxial compression and brittle deformation.

### Uniaxial Compressive and Deformation

Uniaxial compression and deformation processes were measured with a TAW 2000 testing machine. The tests were carried out at room temperature. A constant loading rate of 0.2 MPa/s was applied, with the loading controlled by computer. The compression process stopped as soon as rock failure occurred (**Figure 2**).

### Methane Isothermal Adsorption

Methane sorption isotherms were measured for all original (O) and compressive deformed (D) core samples in a pressure range of 0–15 MPa at 30°C. The high-pressure methane sorption measurements were conducted on an ISO 300 isothermal adsorption apparatus under moisture equilibrated conditions, adopting the GB/T 19560-2004 (China National Standard GB) testing standard, which uses a volumetric method as described in detail in a series of publications (Ji et al., 2012, 2014). The moisture equilibrium conditions were accomplished in an evacuated dryer with relative humidity controlled using saturated solutions of $K_2SO_4$. The shale sample was weighed every 24 h until constant. The moisture content of the shale samples was eventually stabilized between 1.26 and 1.68%. On the assumption that gas absorption in organic rich shales follows monolayer adsorbents theory, $CH_4$ adsorption observed in our experiments was modeled by the Langmuir equation. The temperature and pressure accuracies kept within 0.1°C and 0.1 psi, and variation of temperature and pressure was monitored and recorded by computer. By measuring the pressure before and after expansion, the molar number of the gas at different stages were calculated using an appropriate equation of state, and the amount of gas adsorbed at one pressure level could be determined. The isotherm was obtained by repeating these procedures until the measurement at the highest desired pressure was achieved. Assuming that gas absorption in organic rich shales follows the monolayer adsorbents theory, $CH_4$ adsorption observed in our experiments can be expressed by the Langmuir equation. Base on the measured $CH_4$ sorption parameters, we used the

**FIGURE 2 |** Relationships of axial stress-axial strain for all shale samples. All the curves for represents loading to failure. A typical sample of a Longmaxi shale sample S4 and after failure, abundant graptolite fossils can be observed in the fracture plane (bottom left).
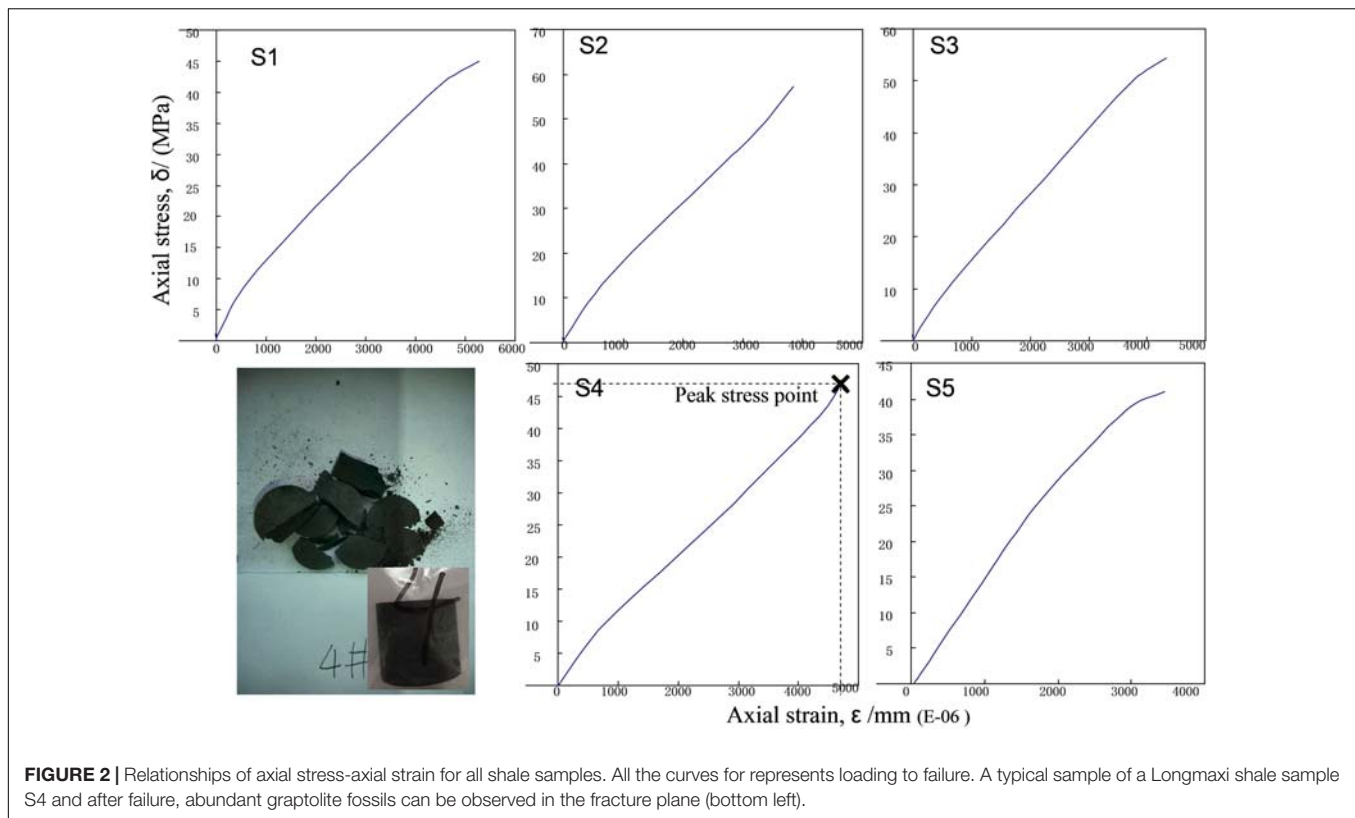
Langmuir equation to describe methane sorption isotherms due to its simplicity and good applicability in fitting the measured data:

$$V = V_L * P/(P_L + P)$$

where V is gas sorption volume per unit weight of shale sample in equilibrium at distinct pressure, $V_L$ is the Langmuir volume (based on monolayer adsorption), which represents the maximum gas sorption capacity at complete surface coverage, P is the gas pressure and $P_L$ is the Langmuir constant, represents the pressure at which total absorbed gas equals to one half of the maximum gas adsorption capacity of Langmuir volume.

## RESULTS AND DISCUSSION

### Shale Composition, Geochemistry and Mineralogy

All samples were either black or dark gray shale, which deposited in deep sea and shallow sea environments (Chen et al., 2011; Liang et al., 2012). The shale composition characteristics of the samples are shown in **Table 1**. Total organic-matter content (TOC%) of the shale samples ranged from 0.17 to 3.05%, while the organic-lean sample has the lowest TOC (0.17%) is a dark gray shale from the upper Longmaxi Formation. The samples are dominated by quartz and clay minerals, accounting for 84–91% of the mass. The clay mineral compositions were mainly the illite/smectite mixed layer and illite (**Table 1**).

The shale of the organic-lean sample has the highest clay mineral content (high illite), but slightly lower quartz content and significant lower TOC than the other samples. However, in general, all shale samples studied were siliceous, with a high brittle mineral content, and the average brittleness index (BRI) was 47.81%.

### Mechanical and Deformation Testing

Ideally, samples for compression experiments should be a perfect cylinder having a length-to-diameter (L/D) ratio of 2.0–2.5 (Brown et al., 1981; ASTM D4543-08, 2008; Fjaer et al., 2008; Dudley et al., 2016). However, it is not always easy to obtain sufficient samples with an L/D ratio exceeding 2, as coring soft shale is frequently difficult, and only 10–20% of the required length may be obtained (Agustawijaya, 2001). In this present study, most of the samples had a L/D ratio of less than 2, which is smaller than the minimum suggested in ISRM guidance (Ulusay and Hudson, 2007). Therefore, the mechanical parameters of uniaxial compressive strength (UCS), Young's modulus (E) or Poisson's ratio (μ) in this article will need to be considered with the above caveat in mind. The mechanical characteristics of the Longmaxi shale are related to its properties of lithology, kerogen and porosity (Zhang et al., 2016). However, as the purpose of this paper is to study changes in methane adsorption capacity before and after compressive deformation, and not the comparative mechanical properties of the Longmaxi shale, we list the mechanical parameters of the samples without further discussion (**Table 2**).

**TABLE 1 |** Geochemical and mineralogical data of the Longmaxi shale samples in this study.

| Sample | Strata | TOC (wt%) | Clay minerals (%) | | | Minerals (%) | | | | | BRI (%) |
|---|---|---|---|---|---|---|---|---|---|---|---|
| | | | C | I | I/S | Clay | Quartz | Carbonate | Feldspar | Pyrite | |
| S1 | $S_1l$ | 0.17 | 18 | 82 | nd | 58 | 32 | nd | 9 | nd | 35.56 |
| S2 | $S_1l$ | 0.93 | 1 | 38 | 61 | 38 | 55 | nd | 7 | nd | 59.14 |
| S3 | $S_1l$ | 0.60 | 15 | 80 | 5 | 47 | 44 | nd | 8 | nd | 48.35 |
| S4 | $S_1l$ | 3.05 | 7 | 39 | 54 | 37 | 49 | 4 | 6 | 4 | 54.44 |
| S5 | $S_1l$ | 0.51 | 9 | 36 | 55 | 47 | 37 | 5 | 9 | 2 | 41.57 |

$S_1l$ – Longmaxi formation, Lower Silurian; TOC – total organic carbon (%); C – Chlorite; I – Illite; I/S – mixed-layer illite/montmorillonite; nd – not detected; BRI – brittleness index, BRI = Quartz/(Quartz + Carbonate + Clay) × 100% (Jarvie et al., 2007).

**TABLE 2 |** Mechanical properties data of shale obtained from uniaxial compressive experiments.

| Sample | Compressive load/P (kN) | Uniaxial compressive strength/σc (MPa) | Elastic modulus/E (GPa) | Poisson's ratio/μ | Comments |
|---|---|---|---|---|---|
| S1 | 25.02 | 45.00 | 9.39 | 0.18 | The loading and compressive process stop when the failure happens, and brittle deformation is formed by sudden failure. |
| S2 | 31.80 | 57.20 | 15.19 | 0.21 | |
| S3 | 31.80 | 57.20 | 15.19 | 0.21 | |
| S4 | 26.07 | 46.90 | 19.94 | 0.23 | |
| S5 | 22.79 | 41.00 | 13.10 | 0.18 | |

Rock failure occurs when loading creates compressive stresses in the sample that exceed the UCS. The failure modes might exhibit brittle or ductile deformation of rock, depending on the brittleness properties of the shale and experimental conditions, such as temperature and pressure. Previous studies have suggested that the Longmaxi formation shale has high brittleness, and thus is suitable for hydraulic fracturing and should readily form complex crack networks (Zhang et al., 2018). Brittle deformation is characterized by sudden failure. **Figure 2** shows a typical sample (θ = 90°) of a Longmaxi shale sample, before and after failure. Abundant graptolite fossils were observed in the fracture plane. **Figure 2** also displays the uniaxial compressive stress-strain diagrams for all 5 shale samples. From these, the approximately linear relationship can be observed before peak stress-strain, with no obvious compaction visible at the initial stage. The linear elastic stage is long, and typical of the brittle characteristics of Longmaxi shale (Zhang et al., 2018). Generally, the failure mode of all 5 samples displayed brittle deformation (**Figure 2**). Similar results have been found in previous studies (Zhang et al., 2018), the brittle mineral content of Longmaxi Formation shale was found to be as high as 72.58% in their report samples, suggested brittle deformation behaviors are closely related to the mineral composition and high brittleness index of the Longmaxi shale sample.

## Methane Adsorption Capacity Measurements

Both the original and artificial deformed shale samples were measured at a temperature of 30°C and pressure up to 15 MPa, under moisture equilibrated condition. Methane sorption capacity varied in the different shale samples. The $CH_4$ sorption capacity is affected by the organic content of the shale. **Figure 3** shows that the measurement adsorption volume of the two highest TOC% shale samples (S4 = 3.05% and S2 = 0.93%) were always higher than that of other organic-poor shale samples (TOC < 0.6%), regardless of compression and deformation, and under all pressure conditions (**Figure 3** and **Table 3**). For the three organic-poor samples, the effect of TOC on $CH_4$ adsorption capacity was not obvious. Sample S1, with the lowest organic matter content (TOC = 0.17%), has a larger adsorption capacity than the other two samples S3 and S5 (0.60 and 0.51% TOC, respectively), which may be related to Sample S1 having the highest clay mineral content (58%), indicating that the clay minerals also contribute toward methane adsorption (Ji et al., 2012; Zhang et al., 2012).

Measured methane sorption isotherms at different pressure can be fitted to a Langmuir function (**Figure 3** and **Table 4**). The overlap between the Langmuir fit curves and the experimental measurements is good (**Figure 3**). **Table 4** shows that the Langmuir maximum $CH_4$ adsorption capacity varies in the different shale samples, obviously affected by the TOC content. Langmuir maximum $CH_4$ adsorption for the two highest TOC% shale samples (S4 = 3.05% and S2 = 0.93%) were higher than 0.14 mmol/g, while the other three organic-lean shale samples were always less than 0.095 mmol/g, with both original and deformed samples (**Table 4**).

## Effect of Compression and Deformation on Methane Gas Adsorption

Measured $CH_4$ sorption capacity is clearly influenced by uniaxial compression and deformation. As shown in **Figure 3**, the $CH_4$ adsorption capacity of all deformed samples was less than of the corresponding original samples, regardless of TOC content and under all $CH_4$ pressures. It shows that compression and the resulting brittle deformation have an effect on the methane adsorption capacity of shale, and the effect is to
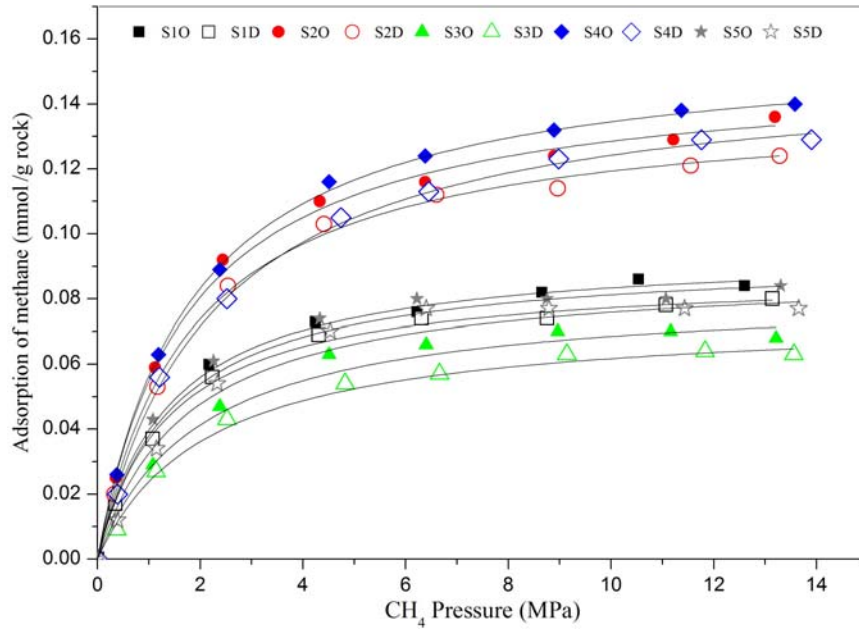
**FIGURE 3 |** Comparison of methane sorption capacity for original shale samples (O) and artificial compressive deformed shale samples (D). Points are experimentally measured results and lines are Langmuir fitting results.

**TABLE 3 |** Measured methane sorption capacity for both original shale samples and deformed samples which after uniaxial compressive experiments.

| S1O | | S2O | | S3O | | S4O | | S5O | |
|---|---|---|---|---|---|---|---|---|---|
| P (MPa) | CH4 (mmol/g rock) | P (MPa) | CH4 (mmol/g rock) | P (MPa) | CH4 (mmol/g rock) | P (MPa) | CH4 (mmol/g rock) | P (MPa) | CH4 (mmol/g rock) |
| 0.00 | 0.000 | 0.00 | 0.000 | 0.00 | 0.000 | 0.00 | 0.000 | 0.00 | 0.000 |
| 0.34 | 0.019 | 0.36 | 0.025 | 0.35 | 0.009 | 0.38 | 0.026 | 0.34 | 0.012 |
| 1.05 | 0.037 | 1.12 | 0.059 | 1.08 | 0.029 | 1.19 | 0.063 | 1.08 | 0.043 |
| 2.17 | 0.060 | 2.44 | 0.092 | 2.38 | 0.047 | 2.38 | 0.089 | 2.26 | 0.061 |
| 4.24 | 0.073 | 4.33 | 0.110 | 4.51 | 0.063 | 4.51 | 0.116 | 4.33 | 0.074 |
| 6.22 | 0.076 | 6.38 | 0.116 | 6.40 | 0.066 | 6.38 | 0.124 | 6.22 | 0.080 |
| 8.65 | 0.082 | 8.89 | 0.124 | 8.96 | 0.070 | 8.89 | 0.132 | 8.75 | 0.080 |
| 10.53 | 0.086 | 11.21 | 0.129 | 11.16 | 0.070 | 11.37 | 0.138 | 11.07 | 0.080 |
| 12.60 | 0.084 | 13.19 | 0.136 | 13.21 | 0.068 | 13.58 | 0.140 | 13.30 | 0.084 |
| S1D | | S2D | | S3D | | S4D | | S5D | |
| 0.00 | 0.000 | 0.00 | 0.000 | 0.00 | 0.000 | 0.00 | 0.000 | 0.00 | 0.000 |
| 0.35 | 0.017 | 0.33 | 0.020 | 0.38 | 0.009 | 0.39 | 0.020 | 0.39 | 0.012 |
| 1.08 | 0.037 | 1.17 | 0.053 | 1.14 | 0.027 | 1.21 | 0.056 | 1.15 | 0.034 |
| 2.24 | 0.056 | 2.54 | 0.084 | 2.52 | 0.043 | 2.52 | 0.080 | 2.33 | 0.054 |
| 4.31 | 0.069 | 4.41 | 0.103 | 4.82 | 0.054 | 4.74 | 0.105 | 4.53 | 0.070 |
| 6.31 | 0.074 | 6.60 | 0.112 | 6.66 | 0.057 | 6.45 | 0.113 | 6.40 | 0.077 |
| 8.76 | 0.074 | 8.96 | 0.114 | 9.14 | 0.063 | 8.98 | 0.123 | 8.79 | 0.077 |
| 11.07 | 0.078 | 11.55 | 0.121 | 11.83 | 0.064 | 11.76 | 0.129 | 11.43 | 0.077 |
| 13.14 | 0.080 | 13.28 | 0.124 | 13.56 | 0.063 | 13.90 | 0.129 | 13.65 | 0.077 |

*Unit conversion factor: 1 mmol/g = 711.24 scf/ton; S4O – shale sample of S4 in Original structure; S4D – shale sample of S4 after compressive.*

reduce the shale adsorption capacity (**Figure 3** and **Table 3**). Similar effects have been found in previous studies of natural geologically deformed shale samples (Zhu et al., 2020). As has

been discussed in previous studies, adsorbed methane capacity positively correlates with the TOC content and clay minerals (Ji et al., 2012, 2014; Zhang et al., 2012). Zhu et al. (2020) conducted

**TABLE 4 |** Langmuir fitting results for methane adsorption for both original shale samples and deformed samples.

| | S1 | | S2 | | S3 | | S4 | | S5 | |
|---|---|---|---|---|---|---|---|---|---|---|
| | Original | Deformed | Original | Deformed | Original | Deformed | Original | Deformed | Original | Deformed |
| Langmuir maximum (mmol/g rock) | 0.095 | 0.088 | 0.151 | 0.141 | 0.082 | 0.075 | 0.159 | 0.152 | 0.093 | 0.089 |
| Langmuir constant (1/MPa) | 1.40 | 1.39 | 1.75 | 1.82 | 1.97 | 2.15 | 1.82 | 2.24 | 1.45 | 1.73 |
| Reduced volume (mmol/g rock) | 0.006 | | 0.010 | | 0.007 | | 0.007 | | 0.004 | |
| Reduced rate (%) | 6.81 | | 6.91 | | 8.48 | | 4.67 | | 4.26 | |

Unit conversion factor: 1 mmol/g = 711.24 scf/ton.

$CH_4$ adsorption measurements for naturally deformed shale samples of both the Lower Silurian Longmaxi Formation and the Lower Cambrian Lujiaping Formation from Chongqing, South China, finding a significant decrease in adsorption capacity for samples that had experienced deformation conditions, ranging from 0.65 to 1.65 $m^3$/t, while those of undeformed samples ranged from 1.44 to 4.56 $m^3$/t. For Longmaxi shale, $CH_4$ adsorption capacity was 0.65 to 1.65 $m^3$/t for naturally deformed samples, while > 2.5 $m^3$/t for undeformed samples, under a $CH_4$ equilibrium pressure of up to 12 MPa (Zhu et al., 2020). This significant decrease (>34%) in the methane adsorption capacity of the naturally deformed Longmaxi shale is much larger than the slight decrease (4.26–8.48%) observed in our present experimental results. This may be due to that there are greater differences in the organic matter and mineral composition between the natural undeformed and deformed samples. On the other hand, it may also be related to the fact that some of the naturally deformed samples in the literature (Zhu et al., 2020) are ductile deformed shale samples, while the influence of ductile deformation on shale pore structure and $CH_4$ adsorption capacity is more significant. These prior studies inferred that volumes of adsorbed methane in the sample suite declined as a result of changes arising during structural deformation.

In the experimental results presented here, the methane adsorption capacity of all deformed samples was less than the corresponding original samples for both the measured results and Langmuir fitted data. The reduced volume amount and reduce rate of the Langmuir maximum adsorption are 0.004–0.010 mmol/g and 4.26–8.48%, respectively. Compared with the dominant effect of TOC on the shale $CH_4$ adsorption capacity, compression and deformation will reduce the adsorption capacity of shale, and the Langmuir maximum adsorption capacity (Qmax) in the samples tested here was reduced from 4.26 to 8.48%. **Figure 4A** shows that compared to clay minerals, the methane sorption capacity of shale has a better positive correlation with TOC, regardless of compression and deformation with both the original (O) samples and deformed (D) samples showing increased $Q_{max}$ with increased TOC. The effect of clay mineral content on $Q_{max}$ is shown in **Figure 4B**. As **Figure 4B** shows, $Q_{max}$ $CH_4$ decreases as the clay content increases, suggesting that clay mineral content is in part responsible for controlling $CH_4$ adsorption. Our results suggest that TOC content is the major controlling factor for $CH_4$ adsorption capacity, agreeing with previous studies

(Ross and Bustin, 2007, 2009; Chalmers and Bustin, 2008a; Zhang et al., 2012).

## Mechanism for Methane Adsorption Reduction in Deformed Samples

The original samples are characterized by well-preserved organic matter pores, interlayer of clay-organic nanocomposites, which may be the possible reason for the higher $CH_4$ adsorption contents (Ma et al., 2020; Zhu et al., 2020). Compressive stress and structure deformation may change the structure of organic matter, the structure of clay minerals (Ma et al., 2020; Zhu et al., 2020), leading to deformation in the microstructure and pore space of the shale matrix (Aplin et al., 2006; Liang et al., 2017; Wang, 2020). Both the previous research on natural deformation samples (Zhu et al., 2020) and the research on artificial compression deformation samples in the present study have shown that compression and structure deformation reduce methane adsorption capacity. The reduction arises from the applied compressive stress and appears related to shale composition, which acts as a higher order control on the amount of $CH_4$ adsorption.

In order to relate the reduction in shale $CH_4$ adsorption capacity to its composition such as TOC and mineral content, the relevant data are plotted in **Figure 5**. Interestingly, unlike the Langmuir $Q_{max}$ value, which is controlled by TOC, the change in $Q_{max}$ for $CH_4$ adsorption has no correlation with either TOC or clay mineral content. In contrast, the reduction in $Q_{max}$ is positively related to the aggregated total of brittle mineral (quartz), OM and clay content ($R^2$ = 0.8748). It suggests that the evolution in pore space and adsorption capacity during compression and deformation are the result of the combined influence of brittle minerals (quartz) and pore providers (OM-clay).

Previous research shows that the pore type in shale is mainly comprised of organic matter pores, intergranular mineral pores, intraparticle mineral pores and microfractures (Loucks et al., 2012). The methane adsorption sites are mainly provided by the surfaces of pores within organic matter, and the surfaces of certain clay minerals (Loucks et al., 2009; Curtis et al., 2012; Ji et al., 2012, 2014; Zhang et al., 2012). Furthermore, the organic matter, clay minerals and quartz all have contact surfaces within the shale matrix. In the original samples, the developed and well-preserved organic

**FIGURE 4 |** **(A)** Relationship between Langmuir maximum sorption capacity and TOC%, **(B)** relationship between Langmuir maximum sorption capacity and Clay%.



**FIGURE 5 |** Relationship between reduced volume of Langmuir maximum sorption capacity and **(A)** TOC%, **(B)** clay%, **(C)** quartz and **(D)** amount content of (TOC + Clay + Quartz)%.
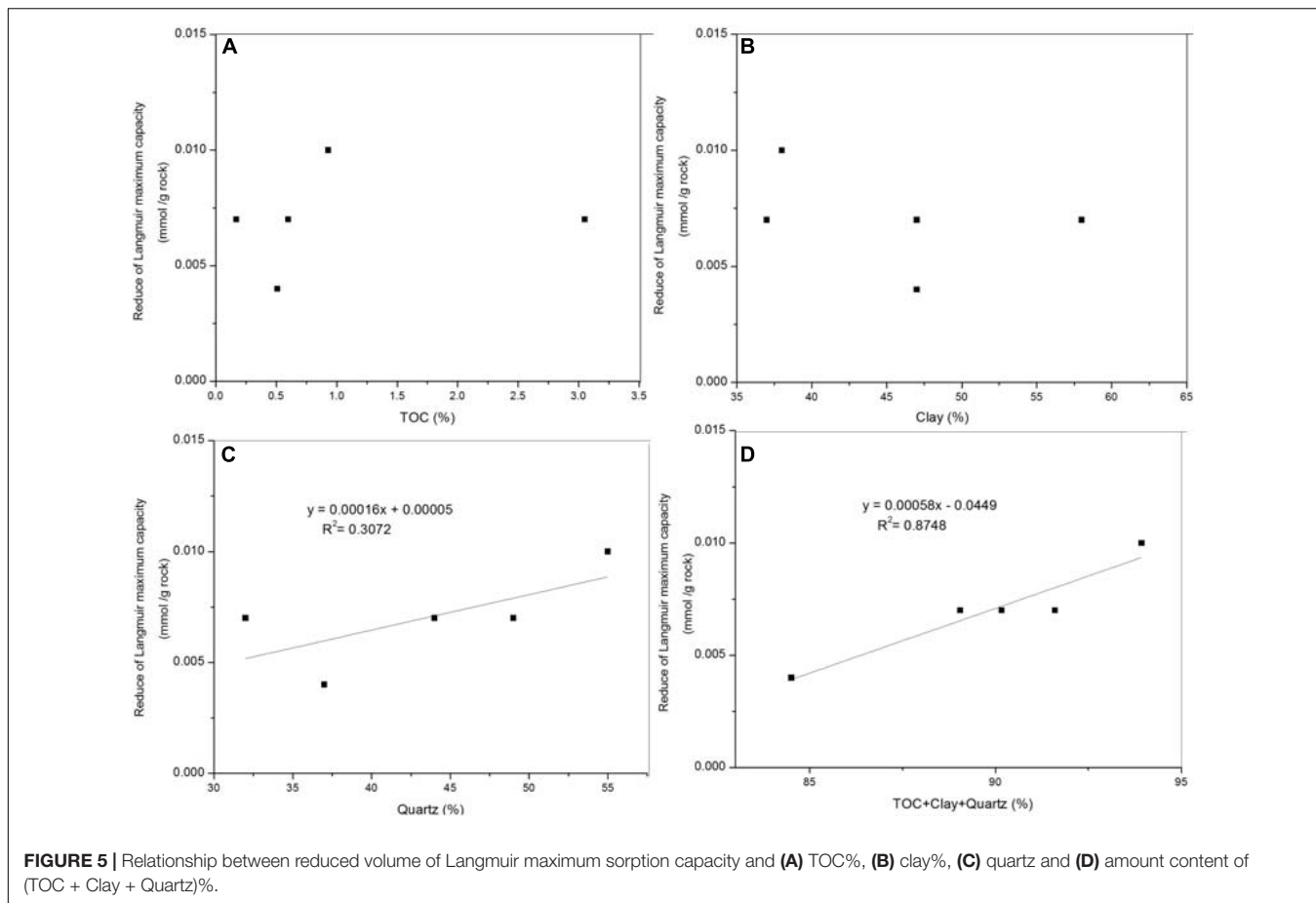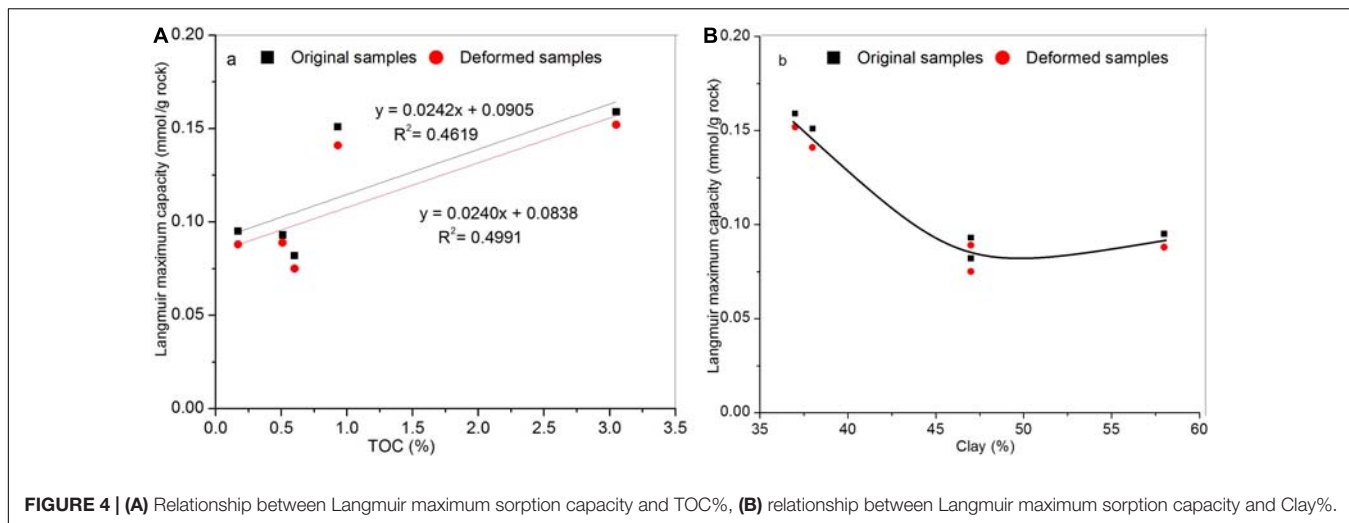
matter pores, along with the interlayer of clay pores may be the reason for the higher $CH_4$ adsorption contents. Under uniaxial compressive condition, brittle minerals of quartz act as stress transmitters, compressing the OM pores and may cause deformation of OM pores (Wang, 2020), changing the pore geometries of organic matter. However, due to the high brittleness characteristics of the Longmaxi Formation

shale, the stress transmission will not be applied indefinitely. When the compressive stress exceeds the UCS of the sample, the compression effect will ending with damage and brittle deformation of shale, thereby retaining parts of OM pores (Wang, 2020). Methane adsorption of shale is related to the specific surface area of the pores (Javadpour et al., 2007; Ross and Bustin, 2009), we also obtained the BET specific surface area

and the external surface area of three shale samples before and after compressive tests using the $N_2$ adsorption method and CT method (**Table 5**). The results show that the external surface area of the damaged shale increases while the internal pore surface area decreases. This may be a reason for the decrease in methane adsorption for deformed shale samples. Unfortunately, when designing the experiments, we did not aimed to determine the pore structure and specific surface area evolution with compressive stress deformation but relationships between compressive deformation and methane adsorption. Therefore, we did not obtain more parameters of the pore structures than the bulk surface area of the limited samples. However, the objective of this present study is still achieved. Overall, the result is that compression will reduce the methane adsorption capacity of the shale, but the impact is slight as shown by the reduction in $Q_{max}$ ranging between 4.26 and 8.48% in this present study.

## Implication of Compression and Deformation Affecting Methane Adsorption

Generally, shale gas is mainly stored as free gas in the meso- to macro-pores and micro-cracks, and as adsorbed gas at the surfaces of nanopores associated with organic matters and clay minerals (Javadpour et al., 2007; Ross and Bustin, 2009). Previous studies indicated that adsorbed gas represents a significant percentage, reaching 20–85% of total gas, which cannot be ignored when evaluating the resource potential (Lu et al., 1995; Ross and Bustin, 2009; Zhang et al., 2012; Wang et al., 2016). The organic matter content is a high level control on determining the gas adsorption capacity of shale, due to $CH_4$ gas primarily being adsorbed within the OM nanopores in shale (Hill et al., 2007; Mastalerz et al., 2012). Unlike North America, the geological conditions of shale reservoirs in South China are highly complicated due to multi-tectonic movement and, as a result, tectonic stress compression. Recently, the effect of tectonic and structural deformation on reservoir characters has attracted more attention (Ma et al., 2015; Liang et al., 2017; He et al., 2018; Zhu et al., 2020). It has been confirmed that the deformation can affect the nanopores in Longmaxi shale (Liang et al., 2017; He et al., 2018), and even reduced the adsorption capacity of deformed shale (Zhu et al., 2020). Whether and how the structural deformation plays an important role in the

adsorbed gas capacity in the deformed shale is still unclear. In this study, we present an experimental study of uniaxial compression induced brittle deformation and its influence on methane adsorption capacity of shale. The remaining OM-pores surface after compression, provides a significant surface area for adsorbed gas, causing slight impairment of adsorbed gas in artificial deformed samples, which is strongly suggested by the good correlation between Langmuir $Q_{max}$ and TOC (**Figure 4A**). Using cold pressing techniques, (Kuila and Prasad, 2013) conducted artificial compaction experiments of Wyoming montmorillonite powder, suggested that compaction could only results in reduction of macropores of the clays while the micropores were not affected by compression. Brittle minerals change the shape of kerogen but not its specific surface area under compressive stress (Wang, 2020). Meanwhile, high brittle minerals content interrupt the compression process by failure and deformation of shale. Thus, this prevents shale OM pores from disappearing under compressive stress, even though the shales which strongly tectonically deformation as mylonite, micropores still develop in the Cambrian shale, South China (Ma et al., 2015). Furthermore, well-preserved OM pores generated in compressive deformed shale result in good adsorbed gas capacity, suggesting that there may still be good gas potential in the tectonic deformation and siliceous shale distribution zones in South China. However, it should be noted when considering the uniaxial compression test, without confining pressure, this is different from the real geologic conditions, and the present study still has limitations. Further artificial compression deformation experiments closer to geologic temperature and pressure conditions such as high temperature and high pressure triaxial compression experiments are warranted.

## CONCLUSION

Comparative analysis of methane adsorption capacity of both original shale samples from the Longmaxi formation, and artificially deformed shale after uniaxial compression and deformation was conducted in this study. The main conclusions are as follows:

(1) Compression deformation does affect the $CH_4$ adsorption capacity of shale. The $CH_4$ sorption capacity of deformed shale samples is reduced after uniaxial compression and brittle deformation, across all 5 shale samples and at each pressure point tested.
(2) The effect of brittle deformation on the $CH_4$ sorption capacity of shale was limited. The methane adsorption capacity of shale is slight reduced by 4.26–8.48% after brittle deformation under uniaxial compressive.

## DATA AVAILABILITY STATEMENT

The original contributions presented in the study are included in the article/supplementary material, further inquiries can be directed to the corresponding author.

**TABLE 5 |** BET surface area and External surface area of samples before and after uniaxial compressive tests.

| ID | BET surface area ($m^2$/g) | External surface area ($m^2$) |
|---|---|---|
| S1O | 26.7992 | 0.002707 |
| S2O | 28.9569 | 0.002818 |
| S3O | 30.3752 | 0.002833 |
| S1D | 12.2955 | 0.003852 |
| S2D | 17.349 | 0.004641 |
| S3D | 16.4364 | 0.003624 |

# AUTHOR CONTRIBUTIONS

ML and ZW conceived of the presented idea. ML wrote the manuscript with support from GZ and HG. XZ, HL, LZ, XF, and KZ helped supervise the projects. All authors discussed the results and contributed to the final manuscript.

# FUNDING

# ACKNOWLEDGMENTS

# REFERENCES

Agustawijaya, D. S. (2001). *The Development of Design Criteria for Underground Excavations in Coober Pedy Arid Soft Rocks*. Ph D. thesis. Australia: University of South Australia.

Aplin, A. C., Matenaar, I. F., McCarty, D. K., and Van Der Pluijm, A. (2006). Influence of mechanical compaction and clay mineral diagenesis on the microfabric and pore-scale properties of deep-water Gulf of Mexico mudstones. *Clays Clay Miner.* 54, 500–514. doi: 10.1346/CCMN.2006.0540411

Arora, S., and Mishra, B. (2015). Investigation of the failure mode of shale rocks in biaxial and triaxial compression tests. *Int. J. Rock Mech. Min. Sci.* 79, 109–123. doi: 10.1016/j.ijrmms.2015.08.014

ASTM D4543-08. (2008). *Standard Practices For Preparing Rock Core As Cylindrical Test Specimens And Verifying Conformance To Dimensional And Shape Tolerances*. West Conshohocken, PA: American Society for Testing and Materials.

Bakhshian, S., and Hosseini, S. A. (2019). Prediction of CO2 adsorption-induced deformation in shale nanopores. *Fuel* 241, 767–776. doi: 10.1016/J.FUEL.2018.12.095

Brown, E. T., International Society for Rock Mechanics (ISRM)., and Commission on Testing Methods. (1981). *Rock Characterization, Testing and Monitoring, ISRM Suggested Methods*. Oxford: Pergamon Press.

Chalmers, G. R. L., and Bustin, R. M. (2007). The Organic Matter Distribution and Methane Capacity of the Lower Cretaceous Strata of Northeastern British Columbia, Canada. *Int. J. Coal Geol.* 70, 223–239. doi: 10.1016/j.coal.2006.05.001

Chalmers, G. R. L., and Bustin, R. M. (2008a). Lower Cretaceous Gas Shales in Northeastern British Columbia, Part I: geological Controls on Methane Sorption Capacity. *Bull. Can. Pet. Geol.* 56, 1–21. doi: 10.2113/gscpgbull.56.1.1

Chalmers, G. R. L., and Bustin, R. M. (2008b). Lower Cretaceous Gas Shales in Northeastern British Columbia, Part II: evaluation of Regional Potential Gas Resources. *Bull. Can. Pet. Geol.* 56, 22–61. doi: 10.2113/gscpgbull.56.1.22

Chen, C., Sun, J., Zhang, Y., Mu, J., Li, W., and Song, Y. (2020). Adsorption characteristics of CH4 and CO2 in organic-inorganic slit pores. *Fuel* 265:116969. doi: 10.1016/j.fuel.2019.116969

Chen, S., Zhu, Y., Wang, H., Liu, H., Wei, W., and Fang, J. (2011). Characteristics and significance of mineral compositions of Lower Silurian Longmaxi Formation shale gas reservoir in the southern margin of Sichuan Basin. *Acta Pet. Sin.* 32, 775–782.

Cheng, A. L., and Huang, W. L. (2004). Selective Adsorption of Hydrocarbon Gases on Clays and Organic Matter. *Org. Geochem.* 35, 413–423. doi: 10.1016/j.orggeochem.2004.01.007

Curtis, M. E., Sondergeld, C. H., Ambrose, R., and Rai, C. (2012). Microstructural investigation of gas shales in two and three dimensions using nanometer-scale resolution imaging. *AAPG Bull.* 96, 665–677. doi: 10.1306/08151110188

Dudley, J. W., Brignoli, M., Crawford, B. R., Ewy, R. T., Love, D. K., McLennan, J. D., et al. (2016). ISRM Suggested Method for Uniaxial-Strain Compressibility Testing for Reservoir Geomechanics. *Rock Mech. Rock Eng.* 49, 4153–4178. doi: 10.1007/s00603-016-1055-4

Fjaer, E., Holt, R. M., Horsrud, P., Raaen, A. M., and Risnes, R. (2008). *Petroleum Related Rock Mechanics, 2nd Edn.* Boston: Elsevier.

Gao, L., Wang, Z., Liang, M., Yu, Y., and Zhou, L. (2018). Experimental Study of the Relationship Between Particle Size and Methane Sorption Capacity in Shale. *J. Vis. Exp.* 138:57705. doi: 10.3791/57705

Guo, S., Lu, X., Song, X., and Liu, Y. (2017). Methane adsorption characteristics and influence factors of Mesozoic shales in the Kuqa Depression, Tarim Basin, China. *J. Pet. Sci. Eng.* 157, 187–195. doi: 10.1016/j.petrol.2017.07.020

He, J., Wang, J., Yu, Q., Liu, W., Ge, X., Yang, P., et al. (2018). Pore structure of shale and its effects on gas storage and transmission capacity in well HD-1 eastern Sichuan Basin, China. *Fuel* 226, 709–720. doi: 10.1016/j.fuel.2018.04.072

He, Q., Dong, T., He, S., and Zhai, G. (2019). Methane adsorption capacity of marine-continental transitional facies shales: the case study of the Upper Permian Longtan Formation, northern Guizhou Province, Southwest China. *J. Pet. Sci. Eng.* 183:106406. doi: 10.1016/j.petrol.2019.106406

Hill, D. G., Lombardi, T. E., and Martin, J. P. (2004). Fractured Shale Gas Potential in New York. *Northeast. Geol. Environ. Sci.* 26, 57–78.

Hill, R. J., Zhang, E. T., Katz, B. J., and Tang, Y. (2007). Modeling of Gas Generation from the Barnett Shale, Fort Worth Basin, Texas. *AAPG Bull.* 91, 501–521. doi: 10.1306/12060606063

Hou, Y., He, S., Yi, J., Zhang, B., Chen, X., Wang, Y., et al. (2014). Effect of pore structure on methane sorption potential of shales. *Pet. Explor. Dev.* 41, 272–281.

Jarvie, D. M., Hill, R. J., Ruble, T. E., and Pollastro, R. M. (2007). Unconventional shale-gas systems: the Mississippian Barnett Shale of north-central Texas as one model for thermogenic shale-gas assessment. *AAPG Bull.* 91, 475–499.

Javadpour, F., Fisher, D., and Unsworth, M. (2007). Nanoscale Gas Flow in Shale Gas Sediments. *J. Can. Pet. Technol.* 46, 55–61. doi: 10.2118/07-10-06

Jenkins, C., and Boyer, C. I. I. (2008). Coalbed- and Shale-Gas Reservoirs. *J. Pet. Technol.* 60, 92–99. doi: 10.2118/103514-ms

Ji, L. M., Zhang, T. W., Milliken, K. L., Qu, J., and Zhang, X. (2012). Experimental Investigation of Main Controls to Methane Adsorption in Clay-Rich Rocks. *Appl. Geochem.* 27, 2533–2545. doi: 10.1016/j.apgeochem.2012.08.027

Ji, W., Song, Y., Jiang, Z., Wang, X., Bai, Y., and Xing, J. (2014). Geological controls and estimation algorithms of lacustrine shale gas adsorption capacity: a case study of the Triassic strata in the southeastern Ordos Basin, China. *Int. J. Coal Geol.* 134, 61–73. doi: 10.1016/j.coal.2014.09.005

Jiang, Z., Song, Y., Tang, X., Li, Z., Wang, X., Wang, G., et al. (2020). Controlling factors of marine shale gas differential enrichment in southern China. *Pet. Explor. Dev.* 47, 661–673.

Kuila, U., and Prasad, M. (2013). Specific surface area and pore-size distribution in clays and shales. *Geophys. Prospect.* 61, 341–362.

Li, J., Zhou, S., Li, Y., Ma, Y., Yang, Y., and Li, C. (2016). Effect of organic matter on pore structure of mature lacustrine organic-rich shale: a case study of the Triassic Yanchang shale. Ordos Basin, China. *Fuel* 185, 421–431. doi: 10.1016/j.fuel.2016.07.100

Li, T., Tian, H., Xiao, X., Cheng, P., Zhou, Q., and Wei, Q. (2017). Geochemical characterization and methane adsorption capacity of overmature organic-rich Lower Cambrian shales in northeast Guizhou region, southwest China. *Mar. Pet. Geol.* 86, 858–873. doi: 10.1016/j.marpetgeo.2017.06.043

Liang, C., Jiang, Z., Yang, Y., and Wei, X. (2012). Characteristics of shale lithofacies and reservoir space of the Wufeng–Longmaxi Formation, Sichuan Basin. *Pet. Explor. Dev.* 39, 691–698.

Liang, M., Wang, Z., Gao, L., Li, C., and Li, H. (2017). Evolution of pore structure in gas shale related to structural deformation. *Fuel* 197, 310–319. doi: 10.1016/j.fuel.2017.02.035

Liu, C., Yin, G., Li, M., Deng, B., Song, Z., Liu, Y., et al. (2019). Shale permeability model considering bedding effect under true triaxial stress conditions. *J. Nat Gas Sci. Eng.* 68:102908. doi: 10.1016/j.jngse.2019.102908

Loucks, R. G., Reed, R. M., Ruppel, S. C., and Hammes, U. (2012). Spectrum of pore types and networks in mudrocks and a descriptive classification for matrix-related mudrock pores. *AAPG Bull.* 96, 1071–1098. doi: 10.1306/08171111061

Loucks, R. G., Reed, R. M., Ruppel, S. C., and Jarvie, D. M. (2009). Morphology, genesis, and distribution of nanometer-scale pores in siliceous mudstones of the Mississippian Barnett Shale. *J. Sediment. Res.* 79, 848–861. doi: 10.2110/jsr.2009 092

Lu, X.-C., Li, F.-C., and Watson, A. T. (1995). Adsorption Measurements in Devonian Shales. *Fuel* 74, 599–603. doi: 10.1016/0016-2361(95)98364-k

Ma, Y., Ardakani, O. H., Zhong, N., Liu, H., Huang, H., Larter, S., et al. (2020). Possible pore structure deformation effects on the shale gas enrichment: an example from the Lower Cambrian shales of the Eastern Upper Yangtze Platform, South China. *Int. J. Coal Geol.* 217:103349.

Ma, Y., Zhong, N., Li, D., Pan, Z., Cheng, L., and Liu, K. (2015). Organic matter/clay mineral intergranular pores in the Lower Cambrian Lujiaping Shale in the north-eastern part of the upper Yangtze area, China: a possible microscopic mechanism for gas preservation. *Int. J. Coal Geol.* 137, 38–54. doi: 10.1016/j.coal.2014.11.001

Mastalerz, M., Schimmelmann, A., Lis, G. P., Drobniak, A., and Stankiewicz, A. (2012). Influence of Maceral Composition on Geochemical Characteristics of Immature Shale Kerogen: insight from Density Fraction Analysis. *Int. J. Coal Geol.* 103, 60–69. doi: 10.1016/j.coal.2012.07.011

Minaeian, V., Dewhurst, D., and Rasouli, V. (2017). Deformational behaviour of a clay-rich shale with variable water saturation under true triaxial stress conditions. *Geomech. Energy Environ.* 11, 1–13. doi: 10.1016/j.gete.2017.04.001

Mishra, B., and Verma, P. (2015). Uniaxial and triaxial single and multistage creep tests on coal-measure shale rocks. *Int. J. Coal Geol.* 137, 55–65. doi: 10.1016/j.coal.2014.11.005

Psarras, P., Holmes, R., Vishal, V., and Wilcox, J. (2017). Methane and CO2 Adsorption Capacities of Kerogen in the Eagle Ford Shale from Molecular Simulation. *Acc. Chem. Res.* 50, 1818–1828. doi: 10.1021/ACS.ACCOUNTS.7B00003

Ross, D. J. K., and Bustin, R. M. (2007). Shale Gas Potential of the Lower Jurassic Gordondale Member, Northeastern British Columbia, Canada. *Bull. Can. Pet. Geol.* 55, 51–75. doi: 10.2113/gscpgbull.55.1.51

Ross, D. J. K., and Bustin, R. M. (2008). Characterizing the Shale Gas Resource Potential of Devonian-Mississippian Strata in the Western Canada Sedimentary Basin: application of an Integrated Formation Evaluation. *AAPG Bull.* 92, 87–125. doi: 10.1306/09040707048

Ross, D. J. K., and Bustin, R. M. (2009). The Importance of Shale Composition and Pore Structure upon Gas Storage Potential of Shale Gas Reservoirs. *Mar. Pet. Geol.* 26, 916–927. doi: 10.1016/j.marpetgeo.2008.06.004

Tan, J., Hu, C., Lyu, Q., Dick, J. M., Ranjith, P. G., Li, L., et al. (2019). Multi-fractal analysis for the AE energy dissipation of CO2 and CO2+ brine/water treated low-clay shales under uniaxial compressive tests. *Fuel* 246, 330–339. doi: 10.1016/j.fuel.2019.03.008

Tan, J., Weniger, P., Krooss, B., Merkel, A., Horsfield, B., Zhang, J., et al. (2014). Shale Gas Potential of the Major Marine Shale Formations in the Upper Yangtze Platform, South China, Part II: methane Sorption Capacity. *Fuel* 129, 204–218. doi: 10.1016/j.fuel.2014.03.064

Tang, X., Jiang, S., Jiang, Z., Li, Z., He, Z., Long, S., et al. (2019). Heterogeneity of Paleozoic Wufeng-Longmaxi formation shale and its effects on the shale gas accumulation in the Upper Yangtze Region, China. *Fuel* 239, 387–402.

Topór, T., Derkowski, A., Ziemiański, P., Szczurowski, J., and McCarty, D. K. (2017). The effect of organic matter maturation and porosity evolution on

methane storage potential in the Baltic Basin (Poland) shale-gas reservoir. *Int. J. Coal Geol.* 180, 46–56. doi: 10.1016/j.coal.2017.07.005

Ulusay, R., and Hudson, J. A. (eds) (2007). *The Complete Isrm Suggested Methods For Rock Characterization, Testing And Monitoring: 1974-2006*. Ankara: International Society of Rock Mechanics.

Vishal, V., Chandra, D., Bahadur, J., Sen, D., Hazra, B., Mahanta, B., et al. (2019). Interpreting Pore Dimensions in Gas Shales Using a Combination of SEM Imaging, Small-Angle Neutron Scattering, and Low-Pressure Gas Adsorption. *Energy Fuels* 33, 4835–4848. doi: 10.1021/acs.energyfuels.9b00442

Wang, G. (2020). Deformation of organic matter and its effect on pores in mud rocks. *AAPG Bull.* 104, 21–36. doi: 10.1306/04241918098

Wang, Y., Huang, J., Wang, S., Dong, D., Zhang, C., and Guan, Q. (2016). Dissection of two calibrated areas of the Silurian Longmaxi Formation, Changning and Jiaoshiba,Sichuan Basin. *Nat. Gas Geosci.* 27, 423–432.

Wang, Y., and Li, C. (2017). Investigation of the P-and S-wave velocity anisotropy of a Longmaxi formation shale by real-time ultrasonic and mechanical experiments unde uniaxial deformation. *J. Pet. Sci. Eng.* 158, 253–267. doi: 10.1016/j.petrol.2017.08.054

Wang, Y., Li, C., Hao, J., and Zhou, R. (2018). X-ray micro-tomography for investigation of meso-structural changes and crack evolution in Longmaxi formation shale during compressive deformation. *J. Pet. Sci. Eng.* 164, 278–288. doi: 10.1016/j.petrol.2018.01.079

Wei, M., Liu, Y., Liu, J., Elsworth, D., and Zhou, F. (2019). Micro-scale investigation on coupling of gas diffusion and mechanical deformation of shale. *J. Pet. Sci. Eng.* 175, 961–970. doi: 10.1016/J.PETROL.2019.01.039

Wu, Y., Li, J., Ding, D., Wang, C., and Di, Y. (2014). A generalized framework model for the simulation of gas production in unconventional gas reservoirs. *SPE J.* 19, 845–857.

Yang, R., He, S., Hu, Q., Hu, D., Zhang, S., and Yi, J. (2016). Pore characterization and methane sorption capacity of over-mature organic-rich Wufeng and Longmaxi shales in the southeast Sichuan Basin, China. *Mar. Pet. Geol.* 77, 247–261. doi: 10.1016/j.marpetgeo.2016.06.001

Zhang, P., Yang, C., Wang, H., Guo, Y., Xu, F., and Hou, Z. (2018). Stress-strain characteristics and anisotropy energy of shale under uniaxial compression. *Rock Soil Mech.* 39, 2106–2114. doi: 10.16285/j.rsm.2016.1824

Zhang, T., Ellis, G. S., Ruppel, S. C., Milliken, K., and Yang, R. (2012). Effect of OrganicMatter Type and Thermal Maturity on Methane Adsorption in ShaleGas Systems. *Org. Geochem.* 47, 120–131. doi: 10.1016/j.orggeochem.2012.03.012

Zhang, W. H., Fu, L. Y., Zhang, Y., and Jin, W. J. (2016). Computation of elastic properties of 3D digital cores from the Longmaxi shale. *Appl. Geophys.* 13, 364–374. doi: 10.1007/s11770-016-0542-4

Zhu, H., Ju, Y., Huang, C., Chen, F., Chen, B., and Yu, K. (2020). Microcosmic gas adsorption mechanism on clay-organic nanocomposites in a marine shale. *Energy* 197:117256. doi: 10.1016/j.energy.2020.11725

Zou, J., Rezaee, R., Xie, Q., You, L., Liu, K., and Saeedi, A. (2018). Investigation of moisture effect on methane adsorption capacity of shale samples. *Fuel* 232, 323–332. doi: 10.1016/j.fuel.2018.05.167